

# Highly Ordered, Millimeter-Scale, Continuous, Single-Crystalline Graphene Monolayer Formed on Ru(0001)

By Yi Pan, Haigang Zhang, Dongxia Shi, Jiatao Sun, Shixuan Du, Feng Liu, and Hong-jun Gao\*

Since its successful fabrication by cleavage in 2004,<sup>[1,2]</sup> graphene has attracted great interest because of its novel properties<sup>[3–5]</sup> and potential applications.<sup>[6–10]</sup> All the existing fabrication methods,<sup>[1,2,11–18]</sup> however, are limited to producing single- and multilayer graphene up to only a few tens of micrometers in dimension, which sometimes contain defects and impurities or have poor structural ordering. The limitation in sample size and quality hinders the measurement of certain physical properties, and constitutes the bottleneck in building graphene-based electronic devices. Here, a method for fabricating single-layer graphene on a large scale by thermal annealing of a ruthenium single crystal containing carbon is reported. Low-energy electron diffraction (LEED) measurements indicate that the graphene grows to sizes as large as a few millimeters with good long-range order; scanning tunneling microscopy (STM) images show continuity and perfect crystallinity. Analysis of Moiré patterns augmented by first-principles calculations shows that the graphene layer is incommensurate with the underlying Ru(0001) surface, forming an  $N \times N$  superlattice with an average lattice strain of ca. +0.81%. Our findings offer an effective method for producing high-quality single-crystalline graphene for fundamental research, as well as large-scale graphene wafers for device fabrication and integration.

Currently, there are three major methods for fabricating single- and multilayer graphene: micromechanical cleavage, or chemical exfoliation, of highly oriented pyrolytic graphite (HOPG),<sup>[1,2,11,12]</sup> thermal decomposition of SiC,<sup>[13,14]</sup> and epitaxial growth by vapor-phase deposition of hydrocarbons or CO on metal substrates.<sup>[16–18]</sup> These existing methods, however, are limited to producing graphene with small dimensions and/or poor long-range order and crystallinity. Graphene prepared by cleavage and exfoliation of HOPG has a very high crystalline quality as predefined in HOPG, but its size is usually limited to micrometers;<sup>[1,2]</sup> in addition, the productivity of this method is rather low. Graphene layers formed on SiC surfaces usually

contain multiple domains, poor long-range order, and structural defects.<sup>[15]</sup> Vapor-phase deposition on metal substrates most often leads to graphene formation only on a portion of the substrate surface.<sup>[19]</sup> A strong need to develop a graphene-fabrication method that overcomes these limitations remains. In this paper, successful growth of highly ordered single-layer graphene on a Ru(0001) surface with unprecedented sizes of up to a few millimeters with excellent crystallinity will be presented.

The graphene layers were grown on a Ru(0001) surface by thermal annealing. The Ru crystal, whose (0001) surface had been polished to a roughness of less than 0.03 μm, was commercially obtained. It was cleaned ultrasonically in high-purity acetone and ethanol, to remove organic contamination on the surface. After cycles of Argon-ion sputtering in an ultrahigh vacuum chamber, the crystal was annealed as follows: the temperature was slowly raised at a pressure no higher than  $1 \times 10^{-7}$  Pa to 1000 K, where it was maintained for 20 min, after which the sample was slowly cooled to room temperature. After this process, graphene had grown on the crystal surface, as characterized *in situ* by LEED, STM, and Auger electron spectroscopy (AES), and further analyzed *ex situ* using low-temperature scanning tunneling spectroscopy (STS) and X-ray photoelectron spectroscopy (XPS).

Through the cycles of pretreatment in an ultrahigh-vacuum (UHV) chamber, highly ordered clean Ru(0001) surfaces were prepared, as confirmed by the sharp hexagonal ( $1 \times 1$ ) LEED patterns obtained. After annealing, additional diffraction spots began to appear, indicating the formation of the graphene layer on the Ru surface. In order to image the entire surface, the sample was moved continuously, and individual LEED patterns at different locations were obtained across the surface at 1 mm intervals. Figure 1 shows five examples of LEED patterns. The two patterns taken at the sample edges (Fig. 1B and F) show poor additional diffraction spots, indicating that no highly ordered graphene was formed in these areas. The three patterns taken in the inner region of the sample surface (Fig. 1C–E) all show sharp additional spots with the same arrangement, indicating highly ordered single-crystalline graphene had formed at these locations. Specifically, the new diffraction spots are arranged in a hexagonal pattern, with the same orientation as the Ru ( $1 \times 1$ ) spots. This kind of LEED pattern is a typical Moiré pattern that results from the superposition of two structures with different lattice constants and/or orientations.<sup>[20]</sup> From the distances between the spots in the LEED patterns, the ratio of the lattice constant of graphene to that of the Ru(0001) surface was deduced to be about 12:11. The most important finding here is that graphene has formed continuously over a very large area of

[\*] Prof. H.-J. Gao, Y. Pan, H. G. Zhang, Dr. D. X. Shi, J. T. Sun, Dr. S. X. Du  
Institute of Physics, Chinese Academy of Sciences  
Beijing, 100190 (PR China)  
E-mail: hjgao@aphy.iphy.ac.cn

Prof. Feng Liu  
Department of Materials Science & Engineering  
University of Utah  
Salt Lake City, Utah 84112 (USA)

DOI: 10.1002/adma.2008000761

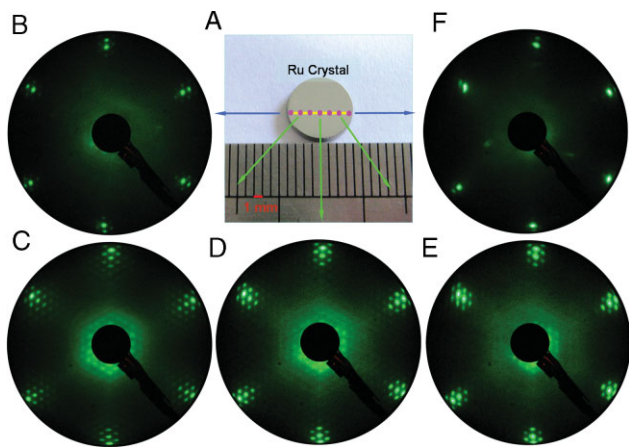


**Figure 1.** LEED patterns obtained from different locations on the sample. A) The sample is a disk of diameter 8 mm, as shown in the photograph. The electron beam was moved along the yellow line to obtain the different LEED patterns. The pink spots are the locations where the photographs shown in (B–F) were taken. In B and F, the additional spots are weak, but in C–E the additional spots are sharp, and have the same arrangement. This indicates that graphene formed at all locations, except at the edges.

several square millimeters on the Ru surface, as indicated by the sharp LEED patterns shown in Figure 1C–E.

To obtain further information about the local surface structure, and to assess the quality and continuity of the graphene layer, STM was used to image the surface; images are shown in Figure 2. Figure 2A shows that the terraces are fully covered by atomically flat graphene. Each terrace is completely covered by a

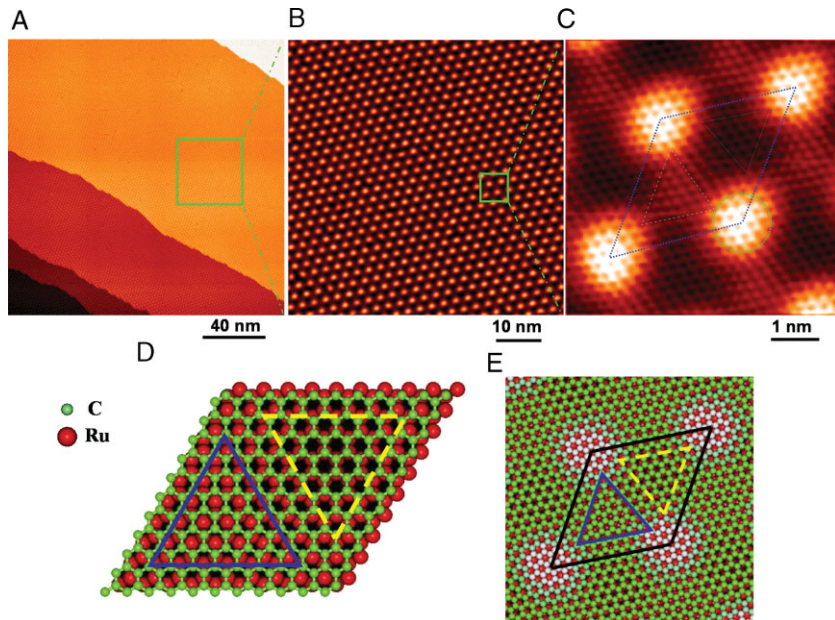


**Figure 2.** STM images of the graphene layer on the Ru(0001) surface. A) The atomically flat graphene flake extended over entire Ru terraces. B) The hexagonal Moiré pattern formed by the superposition of graphene and the Ru substrate. C) Atomic-resolution image of one unit cell of the Moiré pattern. D) Schematic illustration of the optimized atomic structure, showing one unit cell of the superlattice. E) An enlarged perspective view of the superlattice. Tunneling parameters: A) voltage,  $V_s = 1.2$  V, current,  $I = 0.17$  nA; B)  $V_s = -1.2$  V,  $I = 0.35$  nA; and C)  $V_s = -0.46$  V,  $I = 0.27$  nA.

single domain of graphene, and the domains on different terraces are oriented in the same direction. Figure 2B shows a high-resolution image, clearly illustrating the hexagonal Moiré pattern in real space, similar to the results of Ref. [21]. The average distance between the neighboring Moiré spots is 3 nm, that is, 12 times the lattice constant of graphene and 11 times that of Ru. Figure 2C is an image at even higher resolution, showing one unit cell of the Moiré pattern. The graphene overlayer is seen to have a hexagonal instead of honeycomb lattice, because the image has diatomic resolution.<sup>[20]</sup> In this image, 12 graphene atoms can be counted between the centers of the bright Moiré spots, which is consistent with the measurement from Figure 2B.

The lattice mismatch between graphene and the Ru(0001) surface causes the graphene overlayer to have a corrugated surface, producing a strained superlattice with an average in-plane tension of ca. +0.81%. Within each unit cell, the superlattice consists of three structural regions: the bright region (marked by the circle in Fig. 2C) is bowed up into a ridge, the dark region (marked by the dashed triangle in Fig. 2C) is bowed down into a valley, and the intermediate region (marked by the dashed-dotted triangle in Fig. 2C) is of medium height. In the valley region, each atom of the six-member C ring sits right on top of the corresponding Ru atoms underneath, while in the medium-height region the six-member C ring sits on top of one Ru atom.

In support of the experimental studies, a structure model was constructed and first-principles calculations carried out (see Experimental), to determine the ground-state structure of the graphene overlayer on Ru(0001). Figure 2D shows the optimized atomic-structure model with one unit cell of the strained graphene superlattice. Note that in the middle of one half of the cell, the six-member C ring sits right on top of the corresponding Ru atoms, shown within the yellow triangle. In the middle of the other half, the six-member C ring sits on top of one Ru atom, as shown within the blue triangle. This is in agreement with the STM image shown in Figure 2C. Figure 2E shows an enlarged view of one unit cell with color-coded surface heights, illustrating the corrugated nonplanar nature of the graphene surface. The calculated height difference is about 0.4 Å, with the highest regions (colored in white) located at the corner of the cell. This can be compared with the STM image in Figure 2C.

One important finding is that the graphene can form continuously, even over surface steps, without breakage of its structure or symmetry, as shown in Figure 3, suggesting the possibility of growing large-scale graphene with large dimensions. High-resolution STM images were taken over the step-edge areas. Figure 3A shows that the Moiré pattern extends over several terraces, maintaining one single domain of graphene lattice. Figure 3B is an enlarged image of the step edge, which clearly shows that the graphene flake on the upper terrace extends continuously to the lower terrace. Figure 3C shows an atomic-resolution STM image of the step edge, which further

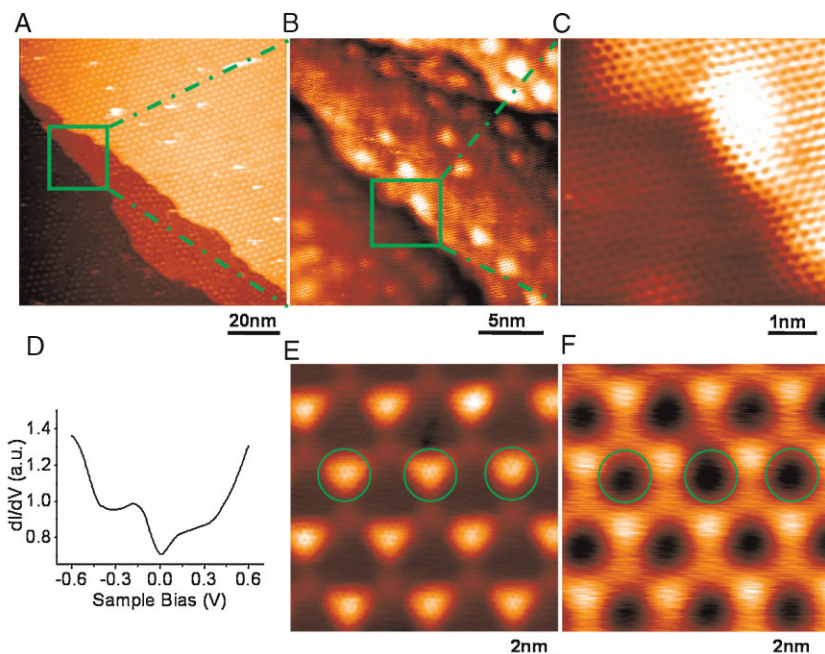


**Figure 3.** STM images of the graphene overlayer above step regions. A) The terraces are continuously covered by graphene, as indicated by the Moiré patterns. B) An enlarged view of the area enclosed by the green rectangle in A), showing the continuous graphene flake on the step edges. C) An atomic-resolution image showing the continuity of the atomic structure and crystallinity of the graphene overlayer across the substrate step edge. D) A  $dI/dV$  spectrum of the graphene layer. It was averaged from dozens of spectra obtained at different locations. STM topography images of graphene on Ru(0001) at voltages of E) 0.5 and F) 3.0 V. Tunneling parameters: A)  $V_s = 2.2$  V,  $I = 0.13$  nA; B)  $V_s = 1.4$  V,  $I = 0.17$  nA; C)  $V_s = 0.2$  V,  $I = 0.43$  nA; E)  $V_s = 0.5$  V; and F)  $V_s = 3.0$  V.

shows that the graphene overlayer remains perfectly crystalline over the step without bond breakage or defects. The crystallinity of the graphene layer, which is continuous over the surface steps, indicates that, even though the substrate terraces are only a few micrometers wide, 2D graphene crystals of much larger dimension (up to millimeters) can form over several terraces. This is found to be the case at least at many steps with single-atomic-layer height; breakage of the graphene overlayer was observed at steps with multi-atomic-layer height.

STS measurements were performed at different locations on the surface. As shown in Figure 3D, a typical semimetal behavior is observed, suggesting that the graphene retains some of its physical properties after being placed on the metal surface. Its density of states near the Fermi level redistributed spatially on the surface due to the corrugation,<sup>[21]</sup> which can be deduced from STM images of the same area taken at different biases, as shown in Figure 3E and F. When the scanning bias was increased from 0.5 to 3 V, the bright areas in Figure 3E marked by the green circles became dark, as shown in Figure 3F. This originated from the interaction between graphene and the metal substrate.

In order to further demonstrate that the graphene layer was composed of carbon, XPS and AES analyses were performed on the sample. It can be seen from the XPS spectrum of Figure 4A that there are two peaks located at 280 and 284.2 eV. These peaks are the Ru 3d<sub>5/2</sub> and 3d<sub>3/2</sub> peaks, respectively; the C 1s (284.7 eV) electron also contributed to the peak at 284.2 eV in the XPS spectrum, implying that the prepared sample may contain carbon. To arrive at a definite conclusion about the carbon on the Ru surface, AES analysis of the sample was conducted. As shown by the black curve in Figure 4B, before formation of the graphene layer, the four peaks located at 150, 200, 230, and 273 eV and their shapes agree very well with the standard Ru AES spectrum. However, after layer formation, the intensity of the peak at 273 eV significantly increased. This increase is attributed to carbon formation on the clean Ru(0001) surface [22]. Therefore, the formed layer is clearly made of carbon, which constitutes the graphene and produces the observed Morié pattern at the Ru(0001) surface, as discussed above.

The growth of a graphene overlayer on the Ru surface is thermodynamically driven by the very large miscibility gap between Ru and C under 2000 °C.<sup>[23]</sup> It was confirmed that the carbon layer was formed by carbon atoms present in the Ru bulk, which segregated from the bulk and accumulated on the surface during the annealing process; any other

possible carbon source was carefully excluded from the UHV chamber. The dimensions, long-range order, and crystallinity of the graphene layer formed depend strongly on the kinetic parameters. If Ru was annealed at the wrong temperature or for an inappropriate time, the 2D hexagonal lattice was less-ordered, and contained a high density of defects and dislocations. Large-scale high-quality graphene could only have been grown under

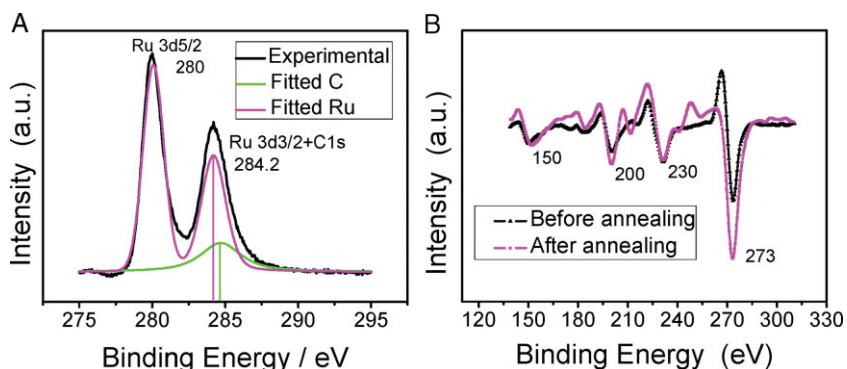


**Figure 4.** XPS and AES spectra of the sample. A) XPS spectrum of the Ru(0001) surface with the graphene adlayer (black curve), which can be decomposed into the standard Ru spectrum (pink curve) and the low-intensity C spectrum (green curve). B) AES spectra of the Ru(0001) surface before (black curve) and after (pink curve) adlayer formation.

the right growth conditions. The appropriate annealing temperature was 1000 K. During initial formation of graphene on the surface, large clusters several nanometers high also formed, as can be seen in the STM images. These amorphous carbon clusters formed everywhere, and covered up to 100% of the graphene surface. They were removed by flash-annealing the crystal in an oxygen atmosphere at 800–1000 K for 50–100 s with an oxygen partial pressure of  $5 \times 10^{-5}$  Pa.

In summary, the formation of a large-scale, highly ordered, single-crystalline continuous monolayer of graphene by thermally annealing a ruthenium single crystal has been presented. The XPS and AES spectra demonstrate that the layer formed is indeed composed of carbon. The Moiré pattern observed by STM was confirmed, with the help of first-principles calculations, to be caused by interference between the lattices of the graphene and the Ru crystal. The graphene grown showed perfect crystallinity, with good long-range order on the order of millimeters and with no bond breakage, even over the substrate steps. It should also be pointed out that, by exposure to ethylene at elevated temperatures in UHV, graphene samples of high quality can also be fabricated on Ru(0001), Ni(111), and Pt(111) crystals. These findings have led to high-quality single-crystalline graphene systems, which can be used for further fundamental research, as well as large-scale graphene wafers, which can be used in device fabrication and integration.

## Experimental

The experiments were carried out in a UHV chamber with a base pressure less than  $1 \times 10^{-8}$  Pa. The chamber was equipped so that room-temperature STM, AES, and LEED could be performed; an electron-beam heating (EBH) stage was also present. The Ru crystal was loaded into the UHV chamber and pretreated using cycles of 0.8 keV Ar<sup>+</sup> sputtering, followed by annealing to 1350 K, until sharp (1 × 1) LEED patterns and clean AES peaks of Ru free from notable impurity peaks were obtained. The temperature was measured using a tungsten-rhenium (W-5%Re/W-26%Re) thermocouple welded to the EBH stage. LEED images were taken using an electron-beam energy of 60 eV. The AES spectra were obtained using an electron-beam energy of 3 kV. XPS analysis was done in a separate chamber. The STS and variable-bias STM images were also taken in a separate chamber, with a low-temperature STM microscope. The crystal with the graphene layer on its surface was taken out of the UHV chamber and protected by high-purity nitrogen in a bag, while being delivered and loaded into the other chambers.

**Computational:** The first-principles calculations were performed using Density Functional Theory (DFT), in which the generalized gradient approximation (GGA) [24,25] for exchange-correlation potentials, the projector-augmented-wave pseudopotential approach, and plane-wave basis set for wavefunction expansion, as implemented in the Vienna Ab-initio Simulation Package (VASP) code [26], were used. The energy cut-off for the plane wave was 400 eV. A slab supercell containing three-layer Ru atoms and monolayer graphene with a vacuum gap of more than 16 Å were used. The graphene and two top metal layers were allowed to relax in structural optimization until the atomic forces relaxed below 0.02 eV Å<sup>-1</sup>. All the calculations were done using experimental Ru lattice constants ( $a = 2.7058$  Å and  $c = 4.2816$  Å).

## Acknowledgements

The work at IOP was supported by grants from the National Science Foundation of China, National "863" and "973" projects of China, the Chinese Academy of Sciences, and Supercomputing Center, CNIC, CAS. Liu is supported by the DOE.

Received: March 18, 2008

Revised: September 22, 2008

Published online:

- [1] K. S. Novoselov, A. K. Geim, S. V. Morozov, D. Jiang, Y. Zhang, S. V. Dubonos, I. V. Grigorieva, A. A. Firsov, *Science* **2004**, *306*, 666.
- [2] K. S. Novoselov, D. Jiang, F. Schedin, T. J. Booth, V. V. Khotkevich, S. V. Morozov, A. K. Geim, *Proc. Natl. Acad. Sci.* **2005**, *102*, 10451.
- [3] K. S. Novoselov, A. K. Geim, S. V. Morozov, D. Jiang, M. I. Katsnelson, I. V. Grigorieva, S. V. Dubonos, A. A. Firsov, *Nature* **2005**, *438*, 197.
- [4] Y. Zhang, J. W. Tan, H. L. Stormer, P. Kim, *Nature* **2005**, *438*, 201.
- [5] T. Nikolaos, J. Csaba, P. Mihaita, T. J. Harry, B. J. van Wees, *Nature* **2007**, *448*, 571.
- [6] J. S. Bunch, A. M. van der Zande, S. S. Verbridge, I. W. Frank, D. M. Tanenbaum, J. M. Parpia, H. G. Craighead, P. L. McEuen, *Science* **2007**, *315*, 490.
- [7] V. V. Cheianov, V. Fal'ko, B. L. Altshuler, *Science* **2007**, *315*, 1252.
- [8] J. R. Williams, L. DiCarlo, C. M. Marcus, *Science* **2007**, *317*, 638.
- [9] D. A. Abanin, L. S. Levitov, *Science* **2007**, *317*, 641.
- [10] Q. Yan, B. Huang, J. Yu, F. Zheng, J. Zang, J. Wu, B. Gu, F. Liu, W. Duan, *Nano Lett.* **2007**, *7*, 1469.
- [11] M. S. Dresselhaus, G. Dresselhaus, *Adv. Phys.* **2002**, *51*, 1.
- [12] A. D. Dmitriy, S. Sasha, J. Z. Eric, D. P. Richard, H. B. Geoffrey, G. E. Dommett, T. N. SonBinh, S. R. Rodney, *Nature* **2007**, *448*, 457.
- [13] I. Forbeaux, J. M. Themlin, J.-M. Debever, *Phys. Rev. B* **1998**, *58*, 16396.
- [14] C. Berger, Z. M. Song, T. B. Li, X. B. Li, A. Y. Ogbazghi, R. D. Feng, Z. T. Dai, A. N. Marchenkov, E. H. Conrad, P. N. First, W. A. de Heer, *J. Phys. Chem. B* **2004**, *108*, 19912.
- [15] G. M. Rutter, J. N. Crain, N. P. Guisinger, T. Li, P. N. First, J. A. Stroscio, *Science* **2007**, *317*, 219.
- [16] R. Rosei, S. Mdesti, F. Sette, C. Q. Quaresima, A. Savoia, P. Perfetti, *Phys. Rev. B* **1984**, *29*, 3416.
- [17] E. V. Rut'kov, A. Y. Tontegonde, *Surf. Sci.* **1985**, *161*, 373.
- [18] T. A. Land, T. Michely, R. J. Behm, J. C. Hemminger, G. Comsa, *Surf. Sci.* **1992**, *264*, 261.
- [19] A. T. N'Diaye, S. Bleikamp, P. J. Feibelman, T. Michely, *Phys. Rev. Lett.* **2006**, *97*, 215501.
- [20] W. T. Pong, C. Durkan, *J. Phys. D: Appl. Phys.* **2005**, *38*, R329.
- [21] a) S. Marchini, S. Günther, J. Winterlin, *Phys. Rev. B* **2007**, *76*, 075429. b) Y. Pan, D. Shi, H. Gao, *Chin. Phys.* **2007**, *16*, 3151.
- [22] R. G. Musket, W. McLean, C. A. Colmenares, D. M. Makowiecki, W. J. Siekhaus, *Appl. Surf. Sci.* **1982**, *10*, 143.
- [23] P. Franke, D. Neuschütz, in *Binary Systems*, Springer, Berlin **2007**, part 5, p. 42.
- [24] J. P. Perdew, J. A. Chevary, S. H. Vosko, K. A. Jackson, M. R. Pederson, D. J. Singh, C. Fiolhais, *Phys. Rev. B* **1992**, *46*, 6671.
- [25] J. P. Perdew, K. Burke, Y. Wang, *Phys. Rev. B* **1996**, *54*, 16533.
- [26] a) G. Kresse, J. Hafner, *Phys. Rev. B* **1993**, *47*, R558. b) G. Kresse, J. Furthüller, *Phys. Rev. B* **1996**, *54*, 11169.